Computers and Mathematics with Applications 69 (2015) 1504–1517

Contents lists available at ScienceDirect

Computers and Mathematics with Applications

journal homepage: www.elsevier.com/locate/camwa

A note on the numerical approach for the reaction–diffusion problem to model the density of the tumor growth dynamics

E. Özuğurlu

Bahçeşehir University, Faculty of Engineering and Natural Sciences, Software Engineering Department, 34353 Beşiktaş, Istanbul, Turkey

ARTICLE INFO

Article history:
Received 6 August 2014
Received in revised form 17 January 2015
Accepted 19 April 2015
Available online 9 May 2015

Keywords:
Glioma growth
Non-linear partial differential equation
Crank–Nicolson method
Brain tumor growth
Proliferation
Reaction–diffusion problem

ABSTRACT

In this article, we numerically solve an equation modeling the evolution of the density of glioma in the brain—the most malignant form of brain tumor quantified in terms of net rates of proliferation and invasion. We employ a non-linear heterogeneous diffusion logistic density model. This model assumes that glioma cell invasion throughout the brain is a reaction–diffusion process and that the coefficient of diffusion can vary according to the gray and white matter composition of the brain at that location. The analysis provided in this article demonstrates that using the correct finite difference scheme can overcome the stability issues caused by the discontinuities of the diffusion coefficient. We also observe that at the steady-state these discontinuities vanish. To visualize and investigate numerically the behavior of the evolution of tumor concentration of the glioma, we calculated and plotted the number of tumor cells, the average mean radial distance, and the speed of the tumor cells along with charting the effects of net dispersal rate and net proliferation rate terms versus time for different center position values of Gaussian initial profile for each zone (gray and white matter tissues). We have proposed two numerical methods, the implicit backward Euler and the averaging in time and forward differences in space (the Crank–Nicolson scheme), both in combination with Newton's method for solving the governing equations. These methods are compared in terms of their performance in varying time-step and mesh-discretization. The Crank–Nicolson implicit method is shown to be the better choice to solve the equation.

1. Introduction

Cancer is a complex disease which leads to the uncontrolled growth of abnormal cells, destruction of normal tissues and invasion of vital organs. Uncontrolled evolution of cells leads to tumor formation but the tumors can be benign and malignant. The distinction between benign and malignant tumors is based on many criteria: degree of differentiation, rate of growth, local invasion and metastatic ability (Prayson [1]).

Mathematical modeling of tumor growth by diffusion has been studied by many researchers (Clatz et al. [2], Cruywagen et al. [3], Glass [4], Rockne et al. [5], Tracqui et al. [6], and Woodward et al. [7]). Unfortunately these works did not consider the spatial heterogeneity of the brain tissue in terms of gray and white matter. Giese et al. [8] experimentally established the result that tumor cells moved faster in white matter than in gray matter. Swanson et al. [9] took into account the spatial heterogeneity of the brain tissue by defining the diffusion coefficient D as a function of the spatial variable differentiating regions of gray and white matter and observed that migration in white brain tissue was faster than in gray tissue.

E-mail address: ersin.ozugurlu@eng.bahcesehir.edu.tr.

http://dx.doi.org/10.1016/j.camwa.2015.04.018
0898-1221/

In a reaction–diffusion model, diffusion and proliferation are the main biological behaviors. This approach models tumor cell infiltration into the surrounding brain tissue. The proliferation is a function representing a reactive behavior and it simulates tumor cell growth and death (Murray [10]). In the literature, the problem of brain tumor growth has been formulated as a reaction–diffusion process, in which the rate of change of tumor cells is given by the net proliferation and diffusion of tumor cells (Bacaër [11], Drasdo [12], Hatzikirou et al. [13], Harpold [14], Mansuri [15], Murray [16], Swanson [17,18]). Swanson's thesis [17] is especially important because it encompasses both the mathematical and medical issues at work. Reaction–diffusion equations with logistic nonlinearity were introduced in the pioneering works of Fisher [19], and Kolmogorov, Petrovskii and Piskunov [20]. The latter model is known as the KPP equation.

Different kinds of cancerous growth such as exponential, logistic and Gompertz are detailed in Murray [16]. Population growth equations are commonly used for the proliferation rate $f(c)$ as summarized either as the exponential law

$$f(c) = \rho\, c(t, x)$$

or the Verhulst (or logistic) law

$$f(c) = \rho\, c(t, x)\left(1 - \frac{c(t, x)}{c_{\max}}\right)$$

or Gompertz law

$$f(c) = -\rho\, c(t, x) \ln\left(\frac{c(t, x)}{e^{k/d}}\right)$$

where ρ is the net proliferation rate in units day^{-1}, $c_{\max}$ represents the carrying capacity of the tissue, providing an upper limit on the number of tumor cells capable of occupying any cubic millimeter of brain, k is the growth rate of tumor and d is a density coefficient, and $e^{k/d}$ is the carrying capacity. Here, k gives an exponential increase when the tumor size $c(t, x)$ is small and d, the decay constant, damps out the growth rate when $c(t, x)$ is large.

The exponential growth is the simplest proliferation law and is suited for quantifying the growth of small tumors during a short period. Gompertz [21] showed that the growth, which was initially exponential, was later limited to an asymptotic rate. In the Gompertzian mode, tumors develop with a growth rate that decreases with the tumoral growth.

The estimation of parameters such as cell proliferation (ρ), diffusion coefficient D, and carrying capacity $c_{\max}$ is important in understanding the behavior of glioma. Since medical imaging techniques can detect regions containing tumor cells, but only if the number of cells are above some threshold (Konukoglu [22]), net rates of proliferation (ρ) and dispersal (diffusion coefficient) D have been estimated from features of pretreatment magnetic resonance (MR) images to predict tumor growth (Tracqui et al. [6], Swanson et al. [9], Powathil et al. [23], Swanson [18], Szeto et al. [24], Konukoglu et al. [25], Roniotis et al. [26]).

The two general numerical methods used to solve the reaction–diffusion equation in the context of tumor growth are finite elements and finite differences. Clatz et al. [27], Hogea et al. [28], and Rockne et al. [29] used finite-element methods to solve anisotropic diffusion equation. But, the finite difference scheme is easier to implement and the pixel structure of digital images provides a natural regular grid. However, the anisotropic diffusion equation is a complex second order partial differential equation (PDE) and simple finite difference is not appropriate. This second order PDE was reduced to simpler first order PDEs by using the concept of manifolds (Cobzas et al. [30] and Konukoglu et al. [25]). But the solution of the equation gives us tumor delineation area instead of the tumor cell density. Jbabdi et al. [31] used chain rule expansion to solve anisotropic diffusion equation, however, Mosayebi et al. [32] proved that chain rule expansion was unstable. In Roniotis [33], anisotropic heterogeneous diffusion case study, the abstract model used was non-linear. However, for their computation, the net cell proliferation rate function was zero which effectively rendered the model linear. They made a detailed error analysis in this linear case. Lolas [34] used finite difference methods to solve isotropic diffusion equation. An isotropic diffusion equation was first proposed by Swanson [17] in her Ph.D. thesis assuming the net growth of glioma cells was linear. Later, Swanson et al. [35], Roniotis et al. [26], Papadomanolaki and Saridakis [36] utilized the finite difference methods to solve heterogeneous version of this diffusion equation.

We should note that tumor environment is combination of many constituents, such as, different types of tumor cells, blood vessels, nutrients, immune system cells, healthy cells, among others. There are numerous researchers modeling the tumor evolution using complex models that have 4-, 6-, and 10-species. For instance, the model developed by Cristini et al. [37] depicted the evolution of the nutrients as a reaction–diffusion equation and delineated the mixture as being composed of tumor cells and water. As the model did not consider the dead cells as a separate constituent, when the cells inside the tumor died because of lack of oxygen, water occupied their original position, and the characteristic necrotic core was not represented. The model developed by Wise et al. [38] splits the tumor into viable and dead cells. This modification allowed the representation of cells dying inside the tumor due to lack of nutrients and oxygen.

The model developed by Hawkins-Daarud et al. [39] was a four-species tumor growth model, in which the extracellular water was divided into nutrient rich and nutrient poor parts. However, it did not reproduce the necrotic core inside the tumor. A universal hybrid 10-species tumor growth model of this general type was recently developed by Lima et al. [40], in which tumor cells were divided into proliferative, hypoxic (quiescent) and necrotic states: healthy cells, nutrient, tumor growth factor and endothelial cells all incorporated in the mixture. Following the work of Lima et al. [40], Lima et al. [41]

developed a system of stochastic partial differential equations governing a six-species tumor growth model accounted for random perturbations that arose from modeling uncertainties in the parameters. They considered an avascular model with six constituents derived directly from the hybrid 10-species model developed in Lima et al. [40] and simulated the stochastic behavior of cellular and macrocellular events affecting the evolution of avascular cancerous tissue using a mixed finite element method and a stochastic collocation scheme.

An extensive review of diffusive modeling of glioma evolution can be found in Roniotis et al. [26], Hatzikirou et al. [13], Giatili and Stamatakos [42], Belmonte-Beitia et al. [43], Branco et al. [44] and references therein.

Recently, in 2014, a book titled by 'Computational Surgery and Dual Training: Computing, Robotics and Imaging' and edited by Garbey et al. [45] was published, and in the Chapter 20 of this book, Sodt et al. [46] employed a finite volume and backward Euler method to discretize the reaction–diffusion equation in 3*D*. They quantitatively compared simulated and actual 3*D* tumor volumes to assess the impact of anisotropic diffusion on the accuracy of their model. By means of a mathematical model for glioma growth, they saw that anisotropic migration of tumor cells along white matter fiber tracts could influence the overall diffusive growth pattern of gliomas.

In this study, our aim is not to discredit the multi species tumor growth models mentioned above but to focus on the methodology of handling stability issues due to the discontinuous diffusion coefficient $D(x)$ in a non-linear heterogeneous diffusion logistic density model.

Our model has been extensively studied (Swanson [17], Swanson et al. [9], and Swanson [47]) and found to be very effective in simulating the behavior of real malignant brain tumors in the time frame for gliomas. The model we are considering in the present work is an analog of this 3-dimensional problem (Sodt et al. [46]) in one spatial dimension.

In this paper, the effects of radiotherapy and chemotherapy are neglected. We adopt a mathematical density model of glioma which assumes that glioma cell invasion throughout the brain is a diffusion process and that the coefficient of diffusion can vary in space depending on the gray and white composition of the brain at that location. In previous studies (Swanson [17,35]) linear growth was considered. Later on, in 2008, Swanson et al. [48] considered logistic growth but with constant diffusion coefficient. We use a non-linear heterogeneous diffusion logistic density model. Unlike Swanson [48], our model is 1-dimensional, however, we assume that the diffusion coefficient D depends on the tissue environment to reflect the observation that glioma cells exhibit higher motility in white matter than in gray matter, thus we consider D as a function of x having a finite number of discontinuities and this results a lack of smoothness in the solution. This is an obstacle for standard numerical procedures, see Section 3.1. However, at the steady-state, these discontinuities vanish.

The formulation and the numerical procedure are described in Sections 2 and 3, respectively. An important question is how the diffusion term is discretized. This is addressed in Section 3.1. The numerical simulations are presented in Section 4.1, the stability condition is derived in Section 4.2, and the analysis is done in Section 4.3. Finally, the conclusion is presented in Section 5.

2. Formulation of the problem

Using parameter ranges obtained from Tracqui et al. [6], along with the evidence that suggests glioma cells migrate with greater velocity through white matter of the brain than through gray (Giese et al. [8]), we extend the model used by Swanson et al. [48] by assuming that the diffusion coefficient D depends on the tissue environment representing the net motility of tumor cells or the Fickian random dispersal rate of glioma cells in undifferentiated brain tissue:

$$\frac{\partial c(t,x)}{\partial t} = \frac{\partial}{\partial x}\left(D(x)\,\frac{\partial c(t,x)}{\partial x}\right) + \rho\, c(t,x)\left(1 - \frac{c(t,x)}{c_{\max}}\right) \tag{2.1}$$

and

$$D(x) = \begin{cases} D_g = 0.13\ \text{mm}^2/\text{day} & 0 \le x \le 7.5 \quad \text{(gray region)} \\ D_w = 0.65\ \text{mm}^2/\text{day} & 7.5 \le x \le 42.5 \quad \text{(white region)} \\ D_g = 0.13\ \text{mm}^2/\text{day} & 42.5 \le x \le 50 \quad \text{(gray region)} \end{cases}$$

(see Fig. 1(b)) with the Neumann boundary conditions (zero-flux)

$$\begin{aligned} c_x(0,t) &= 0 \\ c_x(50,t) &= 0 \end{aligned} \tag{2.2}$$

and the initial condition is taken as Gaussian initial tumor profile (see Fig. 1(a))

$$c(0,x) = g(x) = \frac{1}{\sqrt{2\pi}\,\varepsilon} e^{-\frac{1}{2}\left(\frac{x-x_0}{\varepsilon}\right)^2}, \quad x \in (0,50) \tag{2.3}$$

where $c = c(t,x)$ denoted the tumor concentration of glioma cells at time t and spatial location x and $x_0 = 25$ mm (the middle of the considered interval) and $\varepsilon = 0.01$ suggested by Becker et al. [49]. Here, ρ is the net proliferation rate in units day^{-1} and Fickian diffusion has been used to quantify the random motility of a variety of invading cells (Cozens-Roberts et al. [50]). A factor of 5, $D_w = 5\,D_g$, was used by Swanson et al. [51] but this may vary from patient to patient. The (maximum)

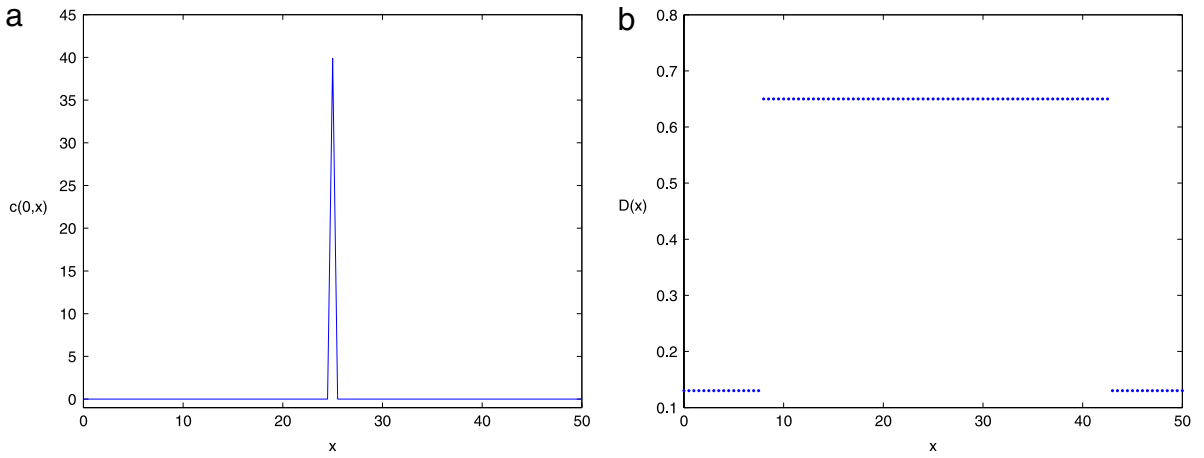

Fig. 1. (a) The initial distribution $c(0,x) = \frac{1}{\sqrt{2\pi}\varepsilon} e^{-\frac{1}{2}\left(\frac{x-x_0}{\varepsilon}\right)^2}$ versus x with $x_0 = 25$ mm (the middle of the considered interval), $\varepsilon = 0.01$, and $\triangle x = 0.5$ mm. (b) The diffusion coefficient $D(x)$ versus x with $\triangle x = 0.5$ mm.

net proliferation rate ρ includes both birth and death rates and assumes logistic growth with a tissue-carrying capacity $c_{\max}$. The net proliferation term includes mitosis, apoptosis, and other cell loss mechanisms. There is a spatial heterogeneity in the net proliferation term resulting from the effect of $c_{\max}$ (Szeto [24]). The model assumes logistic growth of the tumor cell population, so that the net proliferation rate ρ is lower in regions of high cell density (where $c \approx c_{\max}$) than in regions of low cell density (where $c \ll c_{\max}$). As Swanson [17], Harpold et al. [14], Swanson and Alvord [52] suggested, this model served well in capturing tumor dynamics *in vivo* thus far in many iterative comparisons of theory and the real world. This model has proven to be an accurate predictor of simulated tumor growth with respect to anatomical changes that can be imaged by T1-weighted gadolinium enhanced (T1Gd) and T2-weighted MRI (Swanson et al. [47]).

Eq. (2.1) states that tumor cells at a given x either originate from moving to a close location by passive diffusion or from cell division by means of a logistical proliferation model. Eq. (2.1) is a 1-dimensional parabolic partial differential equation. The g function can be considered as the distribution of the initial cell concentration. If the function g is continuous on $[0, 50]$, then the boundary value problem (2.1) has a unique solution.

This model corresponds to the following law: the rate of change of the tumor cell population density is equal to the diffusion of the tumor cells in white and gray matter plus net proliferation of the tumor cells, (Swanson et al. [9]). This PDE (2.1) describes the macroscopic growth and invasion of gliomas under a variety of treatment conditions (Rockne et al. [29], Swanson et al. [53]). Microscopic growth rates describe cell divisions and invasions by means of interactions between tumor cells and their surrounding tissue (Cristini et al. [54], Patel et al. [55]).

Swanson [17] in her Ph.D. thesis used the model given in Eq. (2.1) in order to more accurately reflect the spatial limitation of cellular proliferation and inherent heterogeneity in the brain by allowing the diffusion coefficient D to depend on the tissue environment, $D = D(x)$, however she favored exponential growth for the proliferation rate term $f(c) = \rho\, c(t,x)$. The case of exponential growth $f(c) = \rho\, c(t,x)$ and constant diffusion D was studied (Cruywagen et al. [3], Tracqui et al. [6], Cook et al. [56], Woodward et al. [7], Swanson et al. [9,47], Clatz et al. [27]).

In 2008, Swanson et al. [48] considered logistic growth but with constant diffusion coefficient. Here, we assume that the diffusion coefficient D depends on the tissue environment, namely gray and white matters, thus D is considered as a function of x having finite number of discontinuities and this results in the lack of smoothness in our model solution. This creates a difficulty and is hard to handle with standard numerical procedures, see Section 3.1.

Fickian diffusion has been used to quantify the random motility of a variety of invading cells (Cozens-Roberts et al. [50]) and is implemented in our model to represent the spatial invasion of glioma cells at a rate $D(x)$ which varies depending on the location in the brain to allow for an increased velocity of migration through white matter compared with gray matter. This migration rate in white matter is generally thought to be faster than that in gray matter: $D_w > D_g$ (Giese et al. [8]).

Eqs. (2.1) and (2.2) are solved by applying two different finite-difference methods, namely, implicit backward Euler method and the Crank–Nicolson method.

3. Numerical procedure

3.1. The Chain-rule discretization

It might be tempting to apply the chain rule to rewrite

$$\frac{\partial}{\partial x}\left(D(x)\,\frac{\partial c(t,x)}{\partial x}\right)$$

as

$$\frac{\partial D(x)}{\partial x}\frac{\partial c(t,x)}{\partial x}+D(x)\frac{\partial^2 c(t,x)}{\partial x^2}$$

and then to apply the discretization (Roniotis [33]). However, this is not the best approach as mentioned in Mosayebi et al. [32] in which they proved for 2*D* and 3*D* cases that chain rule expansion violated the stability issues and suggested the directional discretization method which was both theoretically and practically stable if the condition on tensor was satisfied. It is better to discretize the physical problem given in Eq. (2.1) directly. This can be done by first approximating $D(x)\frac{\partial c(t,x)}{\partial x}$ at points halfway between the grid points, using a centered approximation

$$D(x_{i+1/2})\frac{\partial c(x_{i+1/2},t)}{\partial x}=D_{i+1/2}\left(\frac{c_{i+1}-c_i}{\triangle x}\right)$$

and the similar approximation at $x_{i-1/2}$, where $\triangle x=x_{i+1}-x_i$. Subtracting these then gives a centered approximation to

$$\frac{\partial}{\partial x}\left(D(x)\frac{\partial c(t,x)}{\partial x}\right)$$

at the grid point x_i as suggested in LeVeque [57, p. 36]:

$$\begin{aligned}\frac{\partial}{\partial x}\left(D(x)\frac{\partial c(t,x)}{\partial x}\right)&\approx\frac{1}{\triangle x}\left[D_{i+1/2}\left(\frac{c_{i+1}-c_i}{\triangle x}\right)-D_{i-1/2}\left(\frac{c_i-c_{i-1}}{\triangle x}\right)\right]\\&=\frac{1}{(\triangle x)^2}[D_{i-1/2}\,c_{i-1}-(D_{i-1/2}+D_{i+1/2})\,c_i+D_{i+1/2}\,c_{i+1}].\end{aligned}\tag{3.4}$$

3.2. The implicit backward Euler (IBE) method

In this section, we consider an algorithm called the implicit backward Euler method, which results from substituting the backward difference approximation to discretize the PDE (2.1). The spatial domain $[a,b]=[0,50]$ (measured in millimeters) is divided into M sections, each of length $\triangle x=\frac{50}{M}$, $x_i=(i-1)\ \triangle x$ and $i=1,\ldots,M-1$, and each of duration $\triangle t=0.01\approx 14.4$ min. or $\triangle t=0.02\approx 28.8$ min. The implicit backward Euler scheme is applied to Eq. (2.1) using Eq. (3.4), yielding

$$\left(\frac{c_i^{n+1}-c_i^n}{\triangle t}\right)-\left(\frac{D_{i-1/2}\,c_{i-1}^{n+1}-(D_{i-1/2}+D_{i+1/2})\,c_i^{n+1}+D_{i+1/2}\,c_{i+1}^{n+1}}{2(\triangle x)^2}\right)-\frac{\rho}{2}c_i^{n+1}\left(1-\frac{c_i^{n+1}}{c_{\max}}\right)=0.\tag{3.5}$$

The Neumann type of boundary conditions given in Eq. (2.2) are approximated by

$$\frac{c_2^{n+1}-c_0^{n+1}}{2\ \triangle x}=0,\qquad\frac{c_M^{n+1}-c_{M-2}^{n+1}}{2\ \triangle x}=0.$$

Thus, we take $c_0^{n+1}=c_2^{n+1}$ and $c_M^{n+1}=c_{M-2}^{n+1}$. Eq. (3.5) can be rewritten as

$$\frac{\triangle t}{2(\triangle x)^2}\left(D_{i-1/2}\,c_{i-1}^{n+1}-(D_{i-1/2}+D_{i+1/2})\,c_i^{n+1}+D_{i+1/2}\,c_{i+1}^{n+1}\right)+\frac{\triangle t\,\rho}{2}c_i^{n+1}\left(1-\frac{c_i^{n+1}}{c_{\max}}\right)-c_i^{n+1}+c_i^n=0\tag{3.6}$$

where $c_i^n=c(t_n,x_i)=c(n\ \triangle t,i\ \triangle x)$.

We refer this method as *Method IBE*. In Eq. (3.6), c_i^{n+1}, $n=0,\ldots$ and $i=1,\ldots,M-1$ are the unknowns and c_i^0 is the initial data. At each time step, $M-1$ non-linear algebraic equations are solved to find $M-1$ unknowns for fixed values of $D(x)$ and ρ. That system is solved by using Newton's method. The *Method IBE* is first-order accurate in time and second-order accurate in space.

3.3. The Crank–Nicolson (CN) scheme

To have a second-order accurate method in both time and space, the average of the central difference approximations of the spatial derivatives of Eq. (2.1) at the two points $n+1$ and n is taken, yielding

$$\begin{aligned}&\left(\frac{c_i^{n+1}-c_i^n}{\triangle t}\right)-\frac{1}{2}\left(\frac{D_{i-1/2}\,c_{i-1}^{n+1}-(D_{i-1/2}+D_{i+1/2})\,c_i^{n+1}+D_{i+1/2}\,c_{i+1}^{n+1}}{2(\triangle x)^2}\right)\\&-\frac{1}{2}\left(\frac{D_{i-1/2}\,c_{i-1}^{n}-(D_{i-1/2}+D_{i+1/2})\,c_i^{n}+D_{i+1/2}\,c_{i+1}^{n}}{2(\triangle x)^2}\right)-\frac{\rho}{2}\left(\frac{c_i^{n+1}+c_i^n}{2}\right)\left(1-\frac{\left(\frac{c_i^{n+1}+c_i^n}{2}\right)}{c_{\max}}\right)=0\end{aligned}\tag{3.7}$$

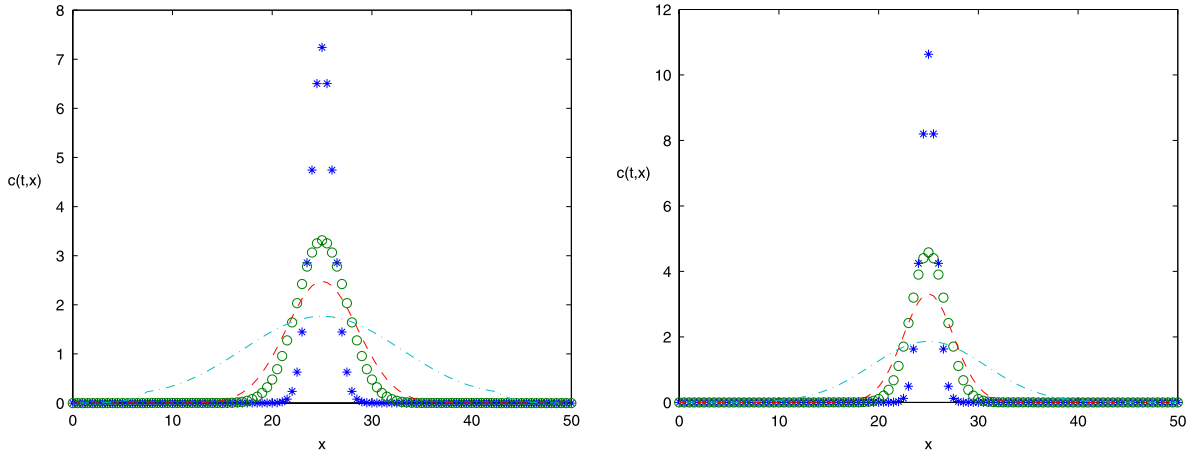

(a) The Crank–Nicolson. (b) The implicit backward Euler.

Fig. 2. The values of the tumor concentration $c(t, x)$ of glioma cells versus x: $\rho = 0.012$ day^{-1}, $\triangle t = 0.01 \approx 14.4$ min., $c_{\max} = 62.5$ cells/mm, $c_0^{\max} = 39.89$ cells/mm and $\triangle x = 0.5$ mm, $t = 1$ (asterisks), $t = 5$ (circles), $t = 10$ days (dashed), and $t = 50$ days (dash–dot).

which leads to the so-called Crank–Nicolson method. We refer this method as *Method CN*. In Eq. (3.7), $c_i^{n+1}, i = 1, \ldots, M-1$ are the unknowns for $n = 0, \ldots$. At each time step, $M-1$ non-linear algebraic equations are solved to find $M-1$ unknowns for fixed values of $D(x)$ and ρ. That system is solved by using Newton's method. The Crank–Nicolson method is second-order accurate in both time and space and unconditionally stable. It is recalled that an algorithm is called numerically stable if an error, whatever its cause, does not grow to be much larger during the calculation.

4. Results and discussion

4.1. Numerical simulations

For all the numerical experiments we describe here, we used 101 spacial grids on $[0, 50]$ with a time step $\triangle t = 0.01$ day ≈ 14.4 min. The CPU time for solving the partial differential equations in 1280×0.01 time steps is about 94 min. with *Method CN* on Linux computer which had an Intel Pentium D 3.00 GHz processor, with 3.50 GB RAM.

Throughout simulations, a five-fold difference in the diffusion coefficients in gray and white matter is used: $D_{white} = 5D_{gray}$ and the growth rate, $\rho = 0.012$ day^{-1} in the model, as suggested for high-grade gliomas by Swanson et al. [48].

All the computational runs are made for $c_{\max} = 62.5$ cells/mm and for

$$c(0, x) = \frac{1}{\sqrt{2\pi}\,\varepsilon} e^{-\frac{1}{2}\left(\frac{x-x_0}{\varepsilon}\right)^2}$$

where $x_0 = 25$ mm (the middle of the considered interval, however we have considered other values of x_0 as well, see Section 4.3.1) and $\varepsilon = 0.01$. The initial distribution $c(0, x)$ has a maximum at $x = x_0$ with a value of $39.89 \approx \frac{1}{\sqrt{2\pi}\,0.01}$ cells/mm, namely $c_0^{\max}$, i.e. we assumed that the tumor has grown to about 39.89 cells/mm as a local density before it begins to diffuse, see Fig. 1(a).

However, the cases of $c_{\max} = 5000$ cells/mm with $c_0^{\max} = 3000$ cells/mm and $c_0^{\max} = 500$ cells/mm have not shown any changes in terms of the graphics but only made a difference on how many days it took to reach the carrying capacity and yielded 1648 days and 1721 days, respectively.

Note that our model shows the tumor cell population reaching a maximum cell number that the tissue can carry, see Figs. 2, 4 and 7(a). However, in reality, after this point, new mutations will continue to occur within the nuclear DNA, providing advantages in their proliferation, survival and invasion.

Fig. 2(a), (b), and Table 1 tell us that the *Method CN* is not only more efficient in terms of errors but also much faster in terms of iteration steps. We can see from Fig. 2(a) and (b) that it takes 1 day for the initial tumor cell concentration to be reduced to 7.24 cells/mm from 39.89 cells/mm in *Method CN*. However, in *Method IBE* this concentration is 10.62 cells/mm. As cells divide, their mutation pattern gives a growth advantage to some of them. This phenomena creates a new subpopulation of cells with higher proliferation rates. As time increases, this subpopulation of cells increases in number within the tumor mass, whereas those cells with lower proliferation rates decrease in number, see Figs. 2, 3 and 6 and Table 1.

Fig. 3 shows the tumor concentration of glioma cells versus x using the *Method CN* on the left and *Method IBE* on the right for $\rho = 0.012$ day^{-1}, $\triangle t = 0.01 \approx 14.4$ min. and $\triangle x = 0.5$ mm, for the time intervals $100 \leq t \leq 200$ and

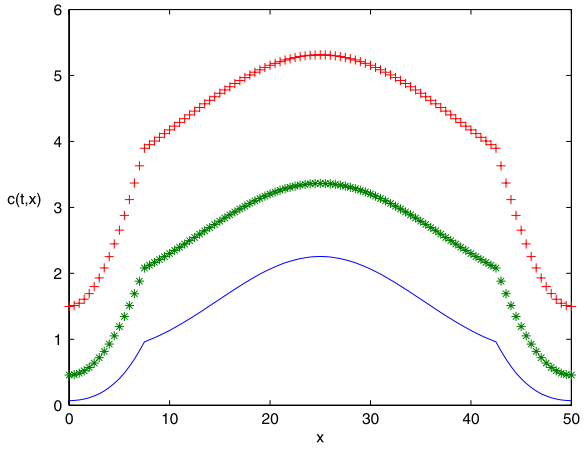

(a) The Crank–Nicolson.

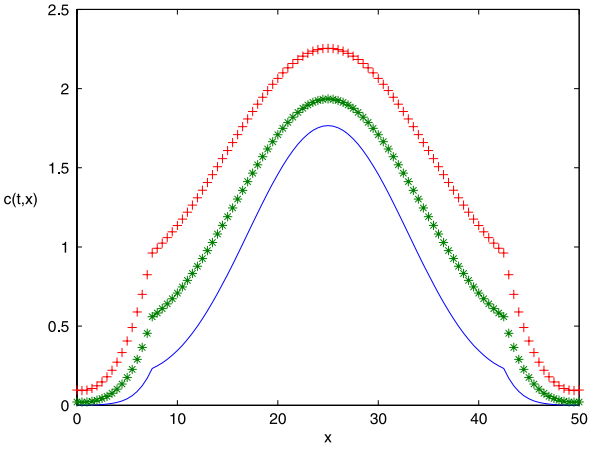

(b) The implicit backward Euler.

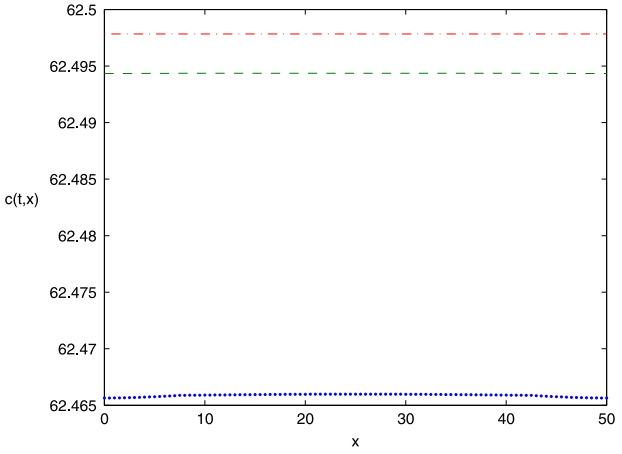

(c) The Crank–Nicolson.

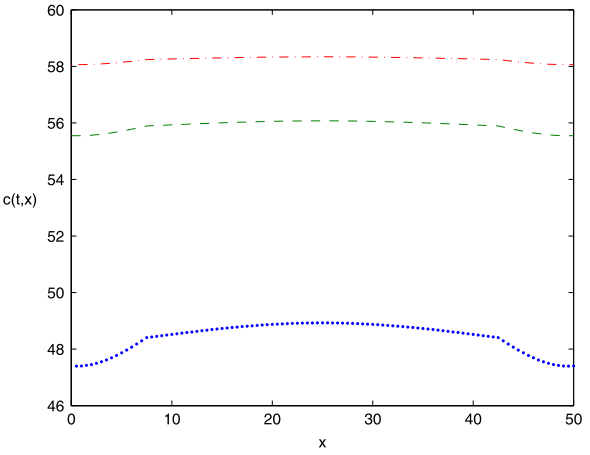

(d) The implicit backward Euler.

Fig. 3. The values of the tumor concentration of glioma cells versus x: $\rho = 0.012$ day^{-1}, $\triangle t = 0.01 \approx 14.4$ min., $c_{\max} = 62.5$ cells/mm, $c_0^{\max} = 39.89$ cells/mm and $\triangle x = 0.5$ mm. (a) and (b) $t = 100$ (solid), 150 (asterisks), and 200 days (plus mark), (c) and (d) $t = 1050$ (dotted), 1200 (dashed), and 1280 days (dash-dot).

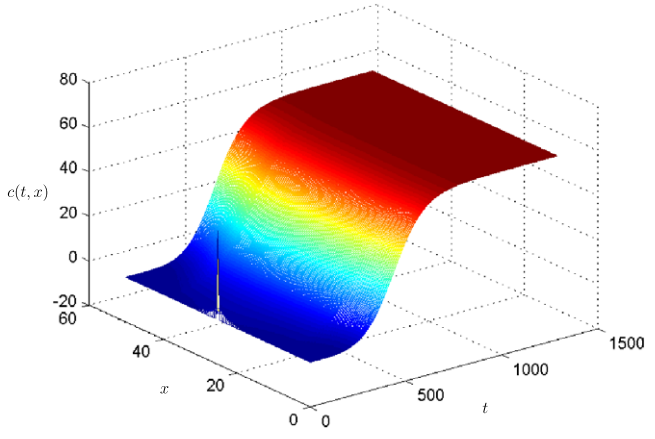

Fig. 4. The evolution of the tumor concentration of glioma cells by using the Crank–Nicolson method: $\rho = 0.012$ day^{-1}, $\triangle t = 0.01 \approx 14.4$ min., $c_{\max} = 62.5$ cells/mm, $c_0^{\max} = 39.89$ cells/mm and $\triangle x = 0.5$ mm, $0 \le x \le 50$, $M = 100$, $0 \le t \le 1280$.

$1050 \le t \le 1280$, respectively. From Fig. 3(a), it can be observed that by $t = 200$ days, the efficiency of the *Method CN* becomes quite obvious since the concentration of the tumor cells reaches 5.2 cells/mm but in *Method IBE* it is 2.25 cells/mm.

Table 1
The typical behavior of the spatial relative error for $\triangle t = 0.01 \approx 14.4$ min. and $\triangle t = 0.02 \approx 28.8$ min., $\triangle x = 0.5$ mm, $c_{\max} = 62.5$ cells/mm, $c_0^{\max} = 39.89$ cells/mm and $\rho = 0.012$ day^{-1}.

Crank–Nicolson		Implicit backward Euler		Time (in days)
l_2-norm	L_∞-norm	l_2-norm	L_∞-norm	
0.4334E−04	0.5781E−04	0.3760E−02	0.5102E−02	1
0.8725E−06	0.1819E−05	0.3558E−03	0.7649E−03	5
0.1621E−06	0.4198E−06	0.1330E−03	0.3645E−03	10
0.4565E−08	0.1132E−07	0.1722E−04	0.6324E−04	50
0.2694E−08	0.4435E−08	0.9755E−05	0.3412E−04	100
0.4333E−08	0.5946E−08	0.1250E−04	0.3121E−04	150
0.6307E−08	0.753E−08	0.1775E−04	0.3488E−04	200
0.7873E−08	0.9123E−08	0.5548E−04	0.5924E−04	400
0.3762E−08	0.5284E−08	0.6446E−04	0.6884E−04	500
0.5713E−09	0.8285E−09	0.7235E−04	0.8146E−04	700
0.1795E−09	0.3235E−09	0.5387E−04	0.7320E−04	800
0.4273E−10	0.1602E−09	0.2557E−04	0.3630E−04	1000
0.2569E−10	0.1601E−09	0.1605E−04	0.2776E−04	1050
0.1503E−10	0.1601E−09	0.1047E−04	0.2061E−04	1100
0.1752E−10	0.1601E−09	0.5041E−05	0.1053E−04	1200
0.0000E+00	0.0000E+00	0.2575E−05	0.5792E−05	1280

It took 114 min. with *Method CN* in 1280 days and with *Method IBE* in 2300 days to reach the maximum capacity $c_{\max} = 62.4989979$ cells/mm, see Fig. 2(c) and (d). In Fig. 2(d), it is plotted only up to 1280 days.

4.2. Stability condition

It can be easily seen that Eq. (2.1) has two stationary states, namely $c(t,x) = 0$ and $c(t,x) = c_{\max}$. As usual it is assumed that the problem is posed on a bounded domain $B \subset R$ with zero flux boundary conditions. Let us evaluate (in an 'energy' sense)

$$\begin{aligned}\frac{d}{dt}\int_B |c(t,x)|^2 dx &= 2\int_B c(t,x)\frac{\partial c(t,x)}{\partial t}dx \\ &= 2\int_B c(t,x)\left[\frac{\partial}{\partial x}\left(D(x)\frac{\partial c(t,x)}{\partial x}\right) + \rho\, c(t,x)\left(1-\frac{c(t,x)}{c_{\max}}\right)dx\right].\end{aligned} \tag{4.8}$$

Using integration by parts as usual and zero-flux conditions for the first integral on the right yields

$$\begin{aligned}\frac{d}{dt}\int_B |c(t,x)|^2 dx &= -2\int_B D(x)\left(\frac{\partial c(t,x)}{\partial x}\right)^2 dx \\ &= 2\rho\int_B (c(t,x))^2\left(1-\frac{c(t,x)}{c_{\max}}\right)dx.\end{aligned} \tag{4.9}$$

Since the diffusion part gives a term with nonnegative sign, we have

$$\begin{aligned}\frac{d}{dt}\int_B |c(t,x)|^2 dx &\le 2\rho\int_B (c(t,x))^2\left(1-\frac{c(t,x)}{c_{\max}}\right) \\ &\le 2\rho\int_B (c(t,x))^2\,dx - 2\rho\int_B \frac{(c(t,x))^3}{c_{\max}}dx \\ &\le 2\rho\int_B (c(t,x))^2\,dx\end{aligned} \tag{4.10}$$

and therefore if $0 < c(0,x) < c_{\max}$ and $\rho > 0$, then $\int_B |c(t,x)|^2 dx$ increases to the carrying capacity $c_{\max}$ exponentially fast by the lemma on Grönwall's inequality, see Figs. 4 and 7(a).

4.3. Analysis

We assume that the diffusion coefficient D depends on the tissue environment, thus we consider D as a function of x having finite number of discontinuities and this results in the lack of smoothness in our model solution. This is an obstacle for standard numerical procedures as we have explained in Section 3.1.

The first two columns of Table 1 clearly show that in *Method CN*, l_2 and L_∞-norms of the spatial relative errors decrease much faster compared to the ones obtained by the *Method IBE*. Unless the stability condition is not violated, the spatial

Table 2
The turning point for different carrying capacities and different initial concentrations, $\triangle t = 0.01 \approx 14.4$ min. and $\rho = 0.012$ day^{-1}.

$\triangle x$ (mm)	$\triangle t$ (day)	$c_{\max}$ (cells/mm)	Peak value of $c(0, x)$	Time at turning point (day)
0.5	0.01	62.5	39.89	42.7
0.5	0.01	5000	500	41.87
0.5	0.01	5000	3000	42.62

relative errors for the *Method IBE* have the same decreasing pattern. Table 1 shows us that *Method CN* is not only more efficient in terms of errors but also much faster in terms of iteration steps. (This is because of its stability and accuracy.)

Table 1 depicts the typical behavior of the spatial relative error in the case of $\triangle x = 0.5$ mm, $\rho = 0.012$ day^{-1} for $\triangle t = 0.01 \approx 14.4$ min. and $\triangle t = 0.02 \approx 28.8$ min. Similar results are obtained by using $\triangle x = 0.25$ mm. For fixed t values, the errors are calculated in different vector norms in order to form a comparison basis:

$$E_{L_\infty} = \frac{\|c_{0.01} - c_{0.02}\|_\infty}{\|c_{0.01}\|_\infty} \quad \text{and} \quad E_{l_2} = \frac{\|c_{0.01} - c_{0.02}\|_2}{\|c_{0.01}\|_2}.$$

Table 2 shows the turning points for each cases of the carrying capacities and the maximum initial tumor concentration of glioma cells. Taking $\triangle t = 0.02 \approx 28.8$ min also yields similar results.

Fig. 4 shows that the tumor concentration of glioma cells, namely, $c(t, x)$, reaches the maximum carrying capacity $c_{\max} = 62.5$ cells/mm which is the size of the stable, steady-state population when $t = 1280$ days by using the *Method CN*.

Fig. 5(a) shows the maximum values of the tumor concentration of glioma cells, $c^*_{\max}(t)$ at each time step versus time for $\triangle t = 0.01 \approx 14.4$ min., $c_{\max} = 5000$ cells/mm and $c_0^{\max} = 3000$ cells/mm and Fig. 5(b) is the zoomed graph of Fig. 5(a) focusing the turning point. As t increases, the tumor concentration of glioma cells reaches the maximum capacity that the tissue can bear. The case for $c_{\max} = 62.5$ cells/mm and $c_0^{\max} = 39.89$ cells/mm gives also a similar result graphically and numerically (an equivalent behavior observed). To verify the numerical methods, simulations have been performed for varying time-step, see Table 1 for $\triangle x = 0.5$ mm.

To understand the effect of each term in our macroscopic reaction–diffusion evolution equation for cancer invasion, we plot the first term (net dispersal of glioma cells) and the second term (net proliferation of glioma cells) on the right-hand side of Eq. (2.1) versus time in days in Fig. 6 for each zone, respectively. It shows that until the day of 105 the net dispersal of glioma cells term is more dominant than net proliferation of glioma cells term in Zones 1 and 3, see Fig. 6(a) and (c), in other words, the tumor heterogeneity is even more noticeable as a result of increased abnormal cell proliferation. Between 105 and 1000 days, net proliferation term dominates the net dispersal term. From Fig. 6, if we look at the data for the total net proliferation and net dispersal of glioma cells, we see that the rate of change of the tumor cell population density increases by $t = 425$ days and then it starts decreasing. This helps us to explain the convexity (concave up) and then concavity (concave down) occurring in the plot of the average number of tumor cells versus time, see Fig. 7.

4.3.1. The average number of tumor cells, the mean radial distance, and the speed of the tumor cells

To gain more insight of the tumor evolution, we also calculated the average number of tumor cells, mean radial distance, and the speed of the tumor cells for each zone and for the whole interval. Now, we define $N(t)$, $L(t)$, and $S(t)$ which have the units of number of cells, the mean radial distance in mm, and the speed in mm/day, respectively, as following: the total number of tumor cells

$$N(t) := \int_0^{50} c(t, x)\, dx,$$

the total mean radial distance of tumor cells

$$L(t) := \frac{\int_0^{50} x\, c(t, x)\, dx}{N(t)},$$

and the total speed of tumor cells $S(t) := \frac{dL(t)}{dt} = \frac{\left[\int_0^{50} x\, \frac{\partial c(t,x)}{\partial t}\, dx - L(t) \int_0^{50} \frac{\partial c(t,x)}{\partial t}\, dx\right]}{N(t)}$.

We can see from Fig. 7(a) that Zone 2 (white region) contributes more to the number of cells since we assume that the tumor has grown to about 19.94 cells as a local mass before it begins to diffuse. Looking at the data plotted in Fig. 7(a), it tells us that in Zone 2, it took nearly 63 days to double the initial tumor cells. By $t = 215$ days, in Fig. 7(a), the tumor cells migrated further into the Zones 1 and 3 in the amount of the initial tumor cells in Zone 2. Additionally, by $t = 218$ days the average number of tumor cells in Zone 2 grew 10 times of the initial tumor cells and 20 times by $t = 289$ days. However, in Zone 1, the average number of tumor cells reached 398 cells by $t = 622$ days and in Zone 3, this was $t = 574$ days. In $t = 631$ days, the average number of cells grew 100 times of the initial tumor cells in Zone 2 (white region), 402 cells, 431 cells for Zone 1 and Zone 3, respectively.

In Fig. 7(b), by $t = 27$ days, the mean radial distance moves 10% to left in Zone 1 and to right 1.69% in Zone 3, just a little bit to left in Zone 2. As time evolves, by $t = 103$ days, in Zone 1 the mean radial distance moves 30% to left but 4.89% to right

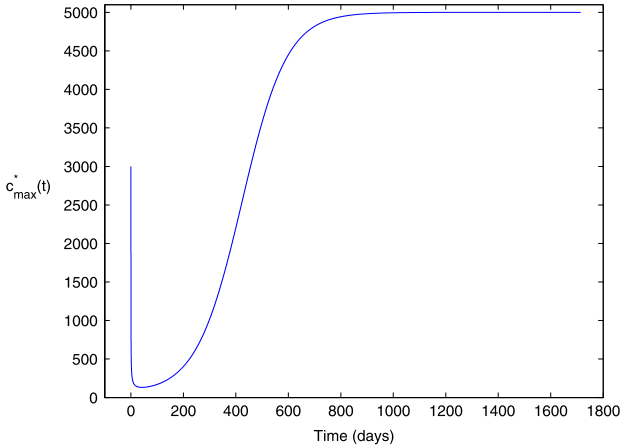

(a) The peaks of concentration versus time.

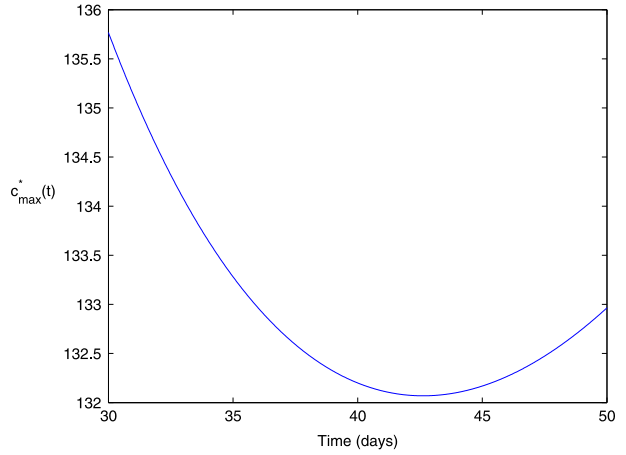

(b) The zoomed graph.

Fig. 5. The maximum values of the tumor concentration $c^*_{\max}(t)$ of glioma cells at each time step versus time: $\rho = 0.012$ day^{-1}, $\triangle t = 0.01 \approx 14.4$ min., $c_{\max} = 5000$ cells/mm, $c_0^{\max} = 3000$ cells/mm and $\triangle x = 0.5$ mm using the Crank–Nicolson method. Fig. 5(b) shows the zoomed graph of Fig. 5(a) around turning point.

Table 3
The Crank–Nicolson Method: the infection days for each zone for different center position x_0 values of Gaussian initial profile (see Eq. (2.3)) for $\triangle t = 0.01 \approx 14.4$ min., $\triangle x = 0.5$ mm, $c_{\max} = 62.5$ cells/mm, $c_0^{\max} = 39.89$ cells/mm and $\rho = 0.012$ day^{-1}.

Gaussian profile position	Infection day		
x_0 (mm)	Zone 1	Zone 2	Zone 3
(Zone 1) 5	–	0.13	37
(Zone 2) 15	1.29	–	17.41
(Zone 2) 25	7.69	–	6.81
(Zone 2) 35	18.83	–	0.98
(Zone 3) 45	39.16	0.22	–

in Zone 3, see also Table 3. Moreover, in Fig. 7(b), the total mean radial distance graph shows that the tumor cells gather at the center of the Zone 2 (white matter), having the radius of 25 mm which means that tumor has occupied the whole tissue finally.

Even though the speed of tumor cells changes sign for each zone, the total speed of tumor cells does not change, see Fig. 7(c). After $t = 800$ days, the total number of tumor cells become constant ($\approx$3090) cells as shown in Fig. 7(a), thus the total speed of tumor cells is zero, see Fig. 7(c).

In all the computational runs, we considered $c_{\max} = 62.5$ cells/mm and took the initial condition as a Gaussian initial tumor profile $c(0, x) = \frac{1}{\sqrt{2\pi}\varepsilon} e^{-\frac{1}{2}\left(\frac{x-x_0}{\varepsilon}\right)^2}$ where $x_0 = 25$ mm (the middle of the considered interval) and $\varepsilon = 0.01$. Table 3

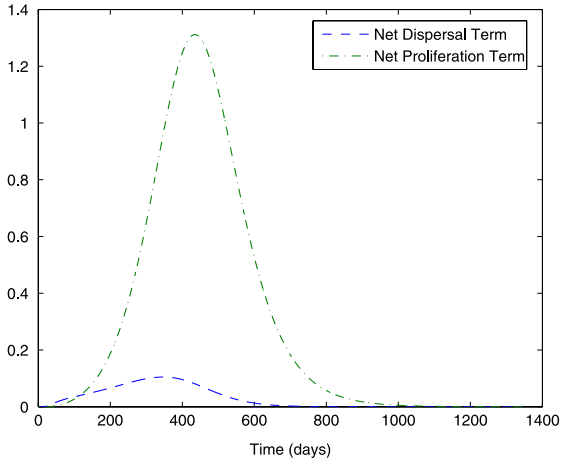

(a) Zone 1 (gray region): $0 \leq x < 7.5$ mm.

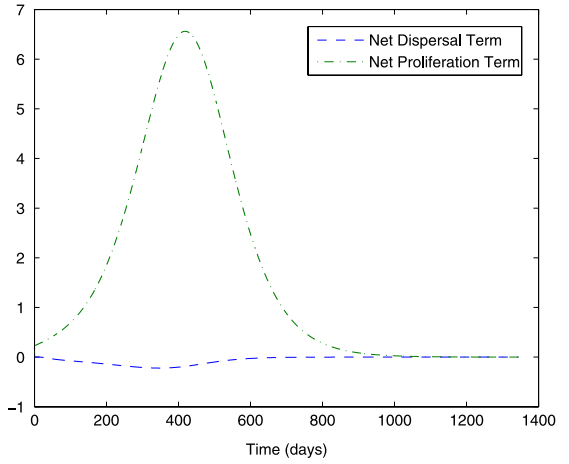

(b) Zone 2 (white region): $7.5 \leq x < 42.5$ mm.

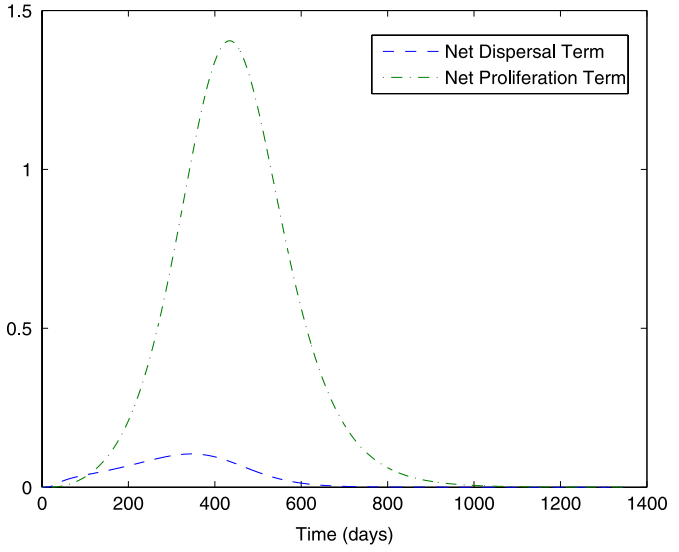

(c) Zone 3 (gray region): $42.5 \leq x < 50$ mm.

Fig. 6. The net dispersal term (DT) and the net proliferation term (PT) of glioma cells versus time in days of Eq. (2.1) for $\rho = 0.012$ day^{-1}, $\triangle t = 0.01 \approx 14.4$ min., $c_{\max} = 62.5$ cells/mm, $c_0^{\max} = 39.89$ cells/mm and $\triangle x = 0.5$ mm.

shows the infected days for each zone for different center position numbers x_0 ranging from 0 to 50. If the center position number $x_0 = 5$, i.e. the center of Gaussian initial profile is located in Zone 1, then the average number of cells for Zone 1 is larger than the one in Zone 3, and the net dispersal term in Zone 1 is more than the one in Zone 3, but as time gets larger they reach an equilibrium value. These observations can be reversed if the center of Gaussian initial profile is located in Zone 3 rather than in Zone 1.

5. Conclusion

In this paper, a mathematical model using one dimensional parabolic equation regarding the growth of human tumors has been presented. What makes this study different from the existing literature is the fact that we check the stability condition and the accuracies of the numerical methods. Since the diffusion coefficient D has a finite number of discontinuities, our model solution has also a lack of smoothness. However, at the steady-state, these discontinuities vanish. Two finite difference methods are employed, namely, the implicit backward Euler method and the Crank–Nicolson method. The Crank–Nicolson implicit method is shown to be the better choice to solve the equation.

Our model shows that tumor cell population reaches a maximum cell number that the tissue can carry, however, in reality, as the cells reach this "steady state", new mutations will continue to occur within the nuclear DNA. These modifications will lead to new phenotypic features of the cancer cell, such as having higher proliferation rates or being more invasive.

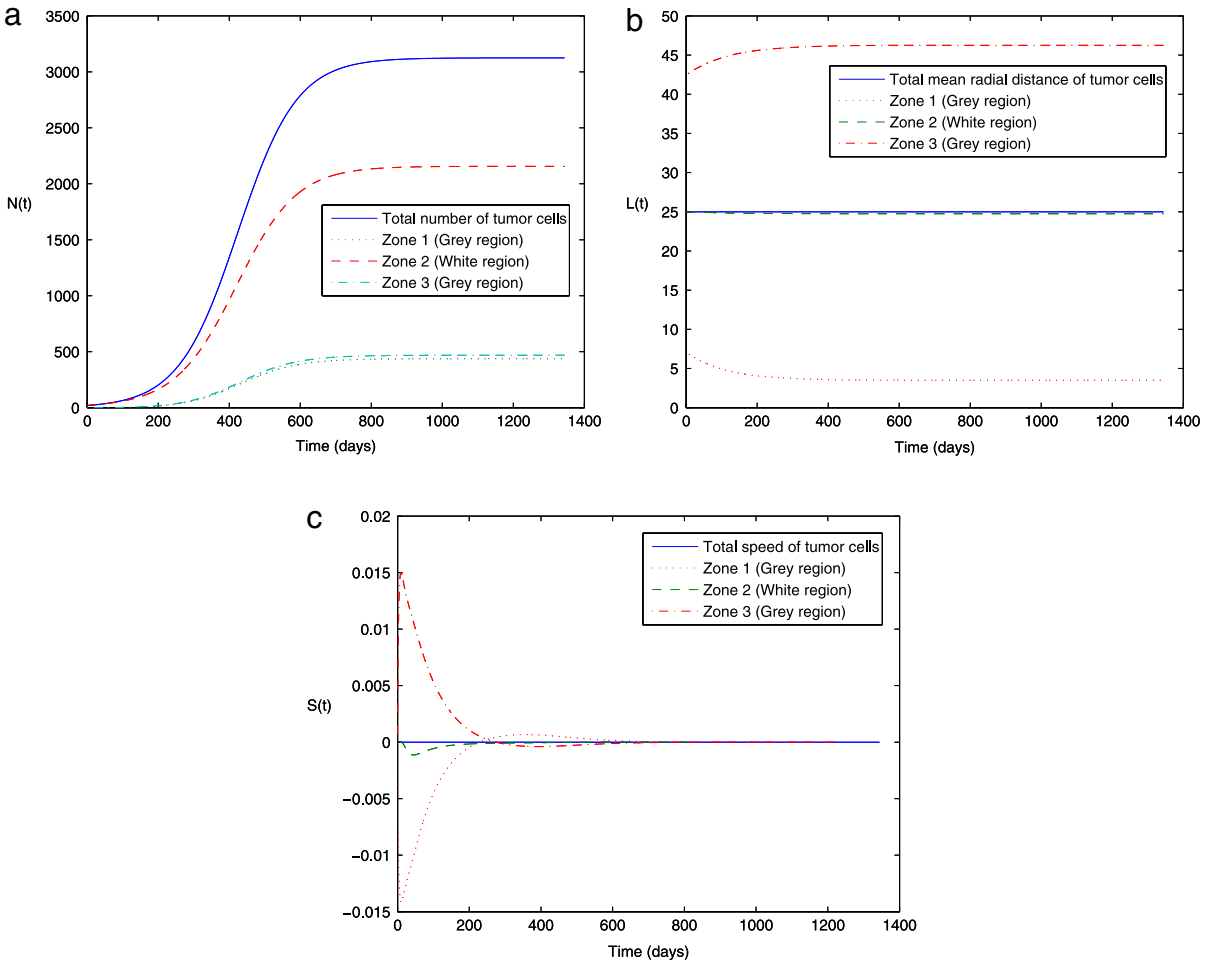

Fig. 7. For each zone: (a) the average number, $N(t)$, of tumor cells, (b) the mean radial distance, $L(t)$, of tumor cells, (c) the speed, $S(t)$, of tumor cells. All these calculations are done for $\rho = 0.012$ day^{-1}, $\triangle t = 0.01 \approx 14.4$ min., $c_{\max} = 62.5$ cells/mm, $c_0^{\max} = 39.89$ cells/mm and $\triangle x = 0.5$ mm.

We have also numerically studied the behavior of the evolution of tumor concentration of the glioma in terms of the number of tumor cells, the average mean radial distance and the speed of tumor cells for different center position values of Gaussian initial profile for each zone.

For future work, we plan to solve the problem in three dimensions by including the radiotherapy and chemotherapy factors. This will help developing ways to integrate data on a patients cancer into personalized models of tumor growth. Such models can better predict how a tumor will respond to different treatments and drugs than any one piece of data alone.

Acknowledgments

The author is grateful for suggestions and comments made by the referees and thanks Gülay Bulut, Devrim Ünay (Bahcesehir University, Turkey), Ender Konukoğlu (Harvard Medical School, USA), Andreas Mang (Luebeck University, Germany), and Maria Papadogiorgaki (Technical University of Creek, Greece) and Victor M. Perez-Garcia Universidad de Castilla-La Mancha, Spain for their constructive comments.

References

[1] R. Prayson, B.K. Kleinschmidt-Demasters, M.D. Cohen, Brain Tumors, Demos Medical Publishing, New York, 2009.
[2] O. Clatz, P.Y. Bondiau, H. Delingette, G. Malandain, M. Sermesant, S. Warfield, N. Ayache, In silico tumor growth: Application to glioblastomas, in: C. Barillot, D.R. Haynor, P. Hellier (Eds.), Proc. of the 7th Int. Conf. on Medical Image Computing and Computer-Assisted Intervention—MICCAI 2004 (2), in: LNCS, vol. 3217, Springer Verlag, Saint-Malo, France, 2004, pp. 337–345.
[3] G.C. Cruywagen, D.E. Woodward, P. Tracqui, G.T. Bartoo, J.D. Murray, E.C. Alvord, The modelling of diffusive tumors, J. Biol. Syst. 3 (4) (1995) 937–945.
[4] L. Glass, Instability and mitotic patterns in tissue growth, J. Dyn. Syst. Meas. Control 95 (1973) 324–327.

[5] R. Rockne, E.C. Alvord, M. Szeto, S. Gu, G. Chakraborty, K.R. Swanson, Modeling Diffusely Invading Brain Tumors An Individualized Approach to Quantifying Glioma Evolution and Response to Therapy, Selected Topics in Cancer Modeling Genesis, Evolution, Immune Competition, and Therapy, Birkhäuser, Boston, 2008.
[6] P. Tracqui, G.C. Cruywagen, D.E. Woodward, G.T. Bartoo, J.D. Murray, E.C. Alvord Jr., A mathematical model of glioma growth: the effect of chemotherapy on spatio-temporal growth, Cell Prolif. 28 (1995) 17–31.
[7] D.E. Woodward, J. Cook, P. Tracqui, G.C. Cruywagen, J.D. Murray, E.C. Alvord Jr., A mathematical model of glioma growth: the effect of extent of surgical resection, Cell Prolif. 29 (1996) 269–288.
[8] A. Giese, L. Kluwe, B. Laube, H. Meissner, M.E. Berens, M. Westphal, Migration of human glioma cells on myelin, Neurosurgery 38 (1996) 755–764.
[9] K.R. Swanson, E.C. Alvord Jr., J.D. Murray, A quantitative model for differential motility of gliomas in grey and white matter, Cell Prolif. 33 (2000) 317–329.
[10] J.D. Murray, Mathematical Biology, Springer-Verlag, Heidelberg, 1989.
[11] N. Bacaër, A Short History of Mathematical Population Dynamics, Springer-Verlag London Limited, 2011.
[12] D. Drasdo, S. Höhme, Individual-based approaches to birth and death in avascular tumors, Math. Comput. Modelling 37 (2003) 1163–1175.
[13] H. Hatzikirou, A. Deutsch, C. Schaller, M. Simon, K.R. Swanson, Mathematical modelling of glioblastoma tumor development: a review, Math. Models Methods Appl. Sci. 15 (11) (2005) 1779–1794.
[14] H.L. Harpold Jr., E.C. Alvord, K.R. Swanson, The evolution of mathematical modeling of glioma proliferation and invasion, J. Neuropathol. Exp. Neurol. 66 (2007) 1–9.
[15] J. Mansuri, The modelling of tumor growth using reaction–diffusion equations (M.Sc. thesis), Oxford University, 2002.
[16] J.D. Murray, Mathematical Biology II: Spatial Models and Biomedical Applications, Springer, New York, NY, 2003.
[17] K.R. Swanson, Mathematical modeling of the growth and control of tumors (Ph.D. thesis), University of Washington, 1999.
[18] K.R. Swanson, Quantifying glioma cell growth and invasion in vitro, Math. Comput. Modelling 47 (2008) 638–648.
[19] Sir R.A. Fisher, The wave of advance of advantageous genes, Ann. Eugenics 7 (1937) 355–369.
[20] A.N. Kolmogorov, I.G. Petrovskii, N.S. Piskunov, A study of the diffusion equation with increase in the amount of substance, and its application to a biological problem, Bull. Moscow Univ. Math. Mech. 1 (6) (1937) 1–26.
[21] B. Gompertz, On the nature of the function expressive of the law of human mortality, and on a new mode of determining the value of life contingencies, Philos. Trans. R. Soc. 115 (1825) 513–585.
[22] E. Konukoglu, Modeling glioma growth and personalizing growth models in medical images (Ph.D. thesis), University of Nice-Sophia Antipolis, 2009.
[23] G. Powathil, M. Kohandel, S. Sivaloganathan, A. Oza, M. Milosevic, Mathematical modeling of brain tumor: Effects of surgery, radiotherapy and chemotherapy, Phys. Med. Biol. 52 (2007) 3291–3306.
[24] M.D. Szeto, G. Chakraborty, J. Hadley, R. Rockne, M. Muzi, E.C. Alvord Jr., K. Krohn, A.M. Spence, K.R. Swanson, Quantitative metrics of net proliferation and invasion link biological aggressiveness assessed by MRI with hypoxia assessed by FMISO-PET in newly diagnosed glioblastomas, Cancer Res. 69 (10) (2009) 4502–4509.
[25] E. Konukoglu, O. Clatz, B.H. Menze, B. Stieltjes, M.-A. Weber, E. Mandonnet, H. Delingette, N. Ayache, Image guided personalization of reaction–diffusion type tumor growth models using modified anisotropic eikonal equations, IEEE Trans. Med. Imaging 29 (1) (2010) 77–95.
[26] A. Roniotis, K. Marias, V. Sakkalis, M. Zerkavis, Diffusive modelling of glioma evolution: a review, J. Biomed. Sci. Eng. 3 (2010) 501–508.
[27] O. Clatz, M. Sermesant, P. Bondiau, H. Delingette, S. Warfield, G. Malandain, N. Ayache, Realistic simulation of the 3D growth of brain tumors in MR images coupling diffusion with mass effect, IEEE Trans. Med. Imaging 24 (10) (2005) 1334–1346.
[28] C. Hogea, F. Abraham, G. Biros, C. Davatzikos, A framework for soft tissue simulations with applications to modeling brain tumor mass-effect in 3D images, in: Proceedings of Medical Image Computing and Computer-Assisted Intervention Workshop on Computational Biomechanics for Medicine, MICCAI, Copenhagen, 2006, pp. 24–33.
[29] R. Rockne, E.C. Alvord Jr., J.K. Rockhill, K.R. Swanson, A mathematical model for brain tumor response to radiation therapy, J. Math. Biol. 58 (4–5) (2009) 561–578.
[30] D. Cobzas, P. Mosayebi, A. Murtha, M. Jagersand, Tumor invasion margin on the Riemannian space of brain fibers, in: Medical Image Computing and Computer-Assisted Intervention—MICCAI 2009, London, UK, Proceedings, Part I, in: Lecture Notes in Computer Science, vol. 5761, Springer, 2009.
[31] S. Jbabdi, E. Mandonnet, H. Duffau, L. Capelle, K. Swanson, M. Pelegrini, R. Guillevin, H. Benali, Simulation of anisotropic growth of low-grade gliomas using diffusion tensor imaging, Magn. Reson. Med. 54 (2005) 616–624.
[32] P. Mosayebi, D. Cobzas, M. Jagersand, A. Murtha, Stability effects of finite difference methods on a mathematical tumor growth model, in: IEEE Computer Society Workshop on Mathematical Methods in Biomedical Image Analysis (MMBIA10) in Conjunction with Computer Vision and Pattern Recognition, CVPR 2010, San Francisco, CA, 2010.
[33] A. Roniotis, V. Sakkalis, I. Karatzanis, M.E. Zerkavis, K. Marias, In–depth analysis and evaluation of diffusive glioma models, IEEE Trans. Inf. Technol. Biomed. 16 (3) (2012) 299–307.
[34] G. Lolas, Mathematical modelling of the urokinase plasminogen activation system and its role in cancer invasion of tissue (Ph.D. thesis), University of Dundee, 2003.
[35] K.R. Swanson, E.C. Alvord Jr., J.D. Murray, Dynamics of a model for brain tumors reveals a small window for therapeutic intervention, Discrete Contin. Dyn. Syst. Ser. B 4 (1) (2004) 289–295.
[36] M.G. Papadomanolaki, Y.G. Saridakis, Collocation with discontinuous Hermite elements for a tumor invasion model with heterogeneous diffusion in 1+1 dimensions, in: Conference in Numerical Analysis, NUMAN2010, Chania, Greece, September 15–18, 2010.
[37] V. Cristini, X. Li, J.S. Lowengrub, S.M. Wise, Nonlinear simulation of solid tumor growth using a mixture model: Invasion and branching, J. Math. Biol. 58 (2009) 723–763.
[38] S.M. Wise, J.S. Lowengrub, H.B. Frieboes, V. Cristini, Three-dimensional multispecies nonlinear tumor growth: I model and numerical method, J. Theoret. Biol. 253 (2008) 524–543.
[39] A. Hawkins-Daarud, K.G. Van Der Zee, J.T. Oden, Numerical simulation of a thermodynamically consistent four-species tumor growth model, Int. J. Numer. Methods Biomed. Eng. 8 (2012) 3–24.
[40] E.A.B.F. Lima, J.T. Oden, R.C. Almeida, A hybrid ten-species phase-field model of tumor growth, Math. Models Methods Appl. Sci. 24 (13) (2014). http://dx.doi.org/10.1142/S0218202514500304.
[41] E.A.B.F. Lima, R.C. Almeida, J.T. Oden, Analysis and numerical solution of stochastic phase-field models of tumor growth, Numer. Methods Partial Differential Equations (2014). http://dx.doi.org/10.1002/num.21934.
[42] S.G. Giatili, G.S. Stamatakos, A detailed numerical treatment of the boundary conditions imposed by the skull on a diffusion–reaction model of glioma tumor growth. Clinical validation aspects, Appl. Math. Comput. 218 (2012) 8779–8799.
[43] J. Belmonte-Beitia, G.F. Calvo, V.M. Pérez-García, Effective particle methods for the Fisher-Kolmogorov equations: Theory and applications to brain tumor dynamics, Commun. Nonlinear Sci. Numer. Simul. 19 (2014) 3267–3283.
[44] J.R. Branco, J.A. Ferreira, Paula de Oliveira, Mathematical modeling of efficient protocols to control glioma growth, Math. Biosci. 255 (2014) 83–90.
[45] M. Garbey, B.L. Bass, S. Berceli, C. Collet, P. Cerveri (Eds.), Computational Surgery and Dual Training: Computing, Robotics and Imaging, Springer, New York, NY, 2014.
[46] R. Sodt, R. Rockne, M.L. Neal, I. Kalet, K.R. Swanson, Quantifying the role of anisotropic invasion in human glioblastoma, in: M. Garbey, B.L. Bass, S. Berceli, C. Collet, P. Cerveri (Eds.), Computational Surgery and Dual Training: Computing, Robotics and Imaging, Springer, New York, NY, 2014, pp. 315–329.
[47] K.R. Swanson, C. Bridge, J.D. Murray, E.C. Alvord Jr., Virtual and real brain tumors: Using mathematical modeling to quantify glioma growth and invasion, J. Neurol. Sci. 216 (1) (2003) 1–10.
[48] K.R. Swanson, R.C. Rostomily, E.C. Alvord Jr., A mathematical modelling tool for predicting survival of individual patients following resection of glioblastoma: a proof of principle, Br. J. Cancer 98 (2008) 113–119.

[49] S. Becker, A. Mang, A. Toma, T.M. Buzug, In-silico oncology: an approximate model of brain tumor mass effect based on directly manipulated free form deformation, Int. J. Comput. Assist. Radiol. Surg. (Int. J. CARS) 5 (6) (2010) 607–622.
[50] C. Cozens-Roberts, J.A. Quinn, D.A. Lauffenburger, Receptor-mediated adhesion phenomena: Model studies with the radial-flow detachment assay, J. Biophys. J. 58 (1990) 107–125.
[51] K.R. Swanson, H.L.P. Harpold, D.L. Peacock, R. Rockne, C. Pennington, L. Kilbride, R. Grant, J.M. Wardlaw, E.C. Alvord Jr., Velocity of radial expansion of contrast-enhancing gliomas and the effectiveness of radiotherapy in individual patients: a proof of principle, Clin. Oncol. 20 (2008) 301–308.
[52] K.R. Swanson, E.C. Alvord Jr., A biomathematical pathological analysis of an untreated glioblastoma, in: NeuroPath. Annual Meeting, Helsinki, Finland, 2002.
[53] K.R. Swanson, E.C. Alvord Jr., J.D. Murray, Quantifying efficacy of chemotherapy of brain tumors with homogeneous and heterogeneous drug delivery, Acta Biotheor. 50 (2002) 223–237.
[54] V. Cristini, J. Lowengrub, Q. Nie, Nonlinear simulation of tumor growth, J. Math. Biol. 46 (3) (2003) 191–224.
[55] A.A. Patel, E.T. Gawlinski, S.K. Lemieux, R.A. Gatenby, A cellular automaton model of early tumor growth and invasion: The effects of native tissue vascularity and increased anaerobic tumor metabolism, J. Theoret. Biol. 213 (3) (2001) 315–331.
[56] J. Cook, D.E. Woodward, P. Tracqui, J.D. Murray, Resection of gliomas and life expectancy, J. Neuro-Oncol. 24 (4) (1995) 131–135.
[57] Randall J. LeVeque, Finite Difference Methods for Ordinary and Partial Differential Equations: Steady-State and Time-Dependent Problems, Society for Industrial and Applied Mathematics (SIAM), Philadelphia, 2007.